LAWRENCE
LIVERMORE
NATIONAL
LABORATORY

LLNL-JRNL-820302

Adjoint Klein-Nishina Sampling Methods: Efficiency, Speed and Applications

A. P. Robinson, D. Henderson, L. Kersting, E. Moll

March 9, 2021

Nuclear Science and Engineering

Disclaimer

Adjoint Klein-Nishina Sampling Methods: Efficiency, Speed and Applications

Alex P. Robinson,[*,a,b] Douglass Henderson,[a] Luke Kersting,[a,c] and Eli Moll[a,d]

[a] *University of Wisconsin - Madison, Department of Nuclear Engineering and Engineering Physics Rm 151 Engineering Research Building 1500 Engineering Drive, Madison, WI 53706-1609*

[b] *Lawrence Livermore National Laboratory, Weapons and Complex Integration B314, R2002, Livermore, CA 94450*

[c] *Sandia National Laboratories, Radiation Effects Theory Department P.O. Box 5800, MS1179, Albuquerque, New Mexico 87185*

[d] *Phoenix, 2555 Industrial Drive, Monona, WI 53713*

[*]Email: robinson124@llnl.gov

Number of pages: 27
Number of tables: 1
Number of figures: 7

Abstract

Three new rejection sampling methods for generating samples from the adjoint Klein-Nishina cross section are discussed: the *two-branch rejection sampling procedure*, the *three-branch linear rejection sampling procedure* and the *three-branch inverse rejection sampling procedure*. These methods have all been implemented in the Framework for REsearch in Nuclear ScIence and Engineering (FRENSIE). The efficiency and sample generation rate of each of these methods are evaluated to characterize the methods and to make recommendations regarding their use. The use of these methods in realistic transport simulations is also evaluated by incorporating a scattering function into the sampling process. The results of an infinite medium problem are presented to verify that the sampling procedure can be used in an adjoint Monte Carlo simulation to generate results that are in agreement with an equivalent forward simulation.

Keywords — Adjoint, Rejection Sampling, Klein-Nishina, Monte Carlo

I. INTRODUCTION

Several Monte Carlo codes have the capability to perform continuous energy adjoint photon transport simulations [1, 2, 3]. While the work to bring the continuous energy adjoint photon transport methods to parity with the forward methods is ongoing, one area that has been neglected is the development of effective sampling methods for the adjoint Klein-Nishina cross section. As will be shown shortly, the complex nature of the adjoint Klein-Nishina cross section compared to its forward counterpart makes it more difficult to construct effective sampling methods. The methods that will be discussed are by no means fully optimized, but they can be used to generate samples efficiently and quickly from the adjoint Klein-Nishina cross section without having to use importance sampling, as is currently done in some codes [2].

The next section of this paper highlights a few important features of the adjoint Klein-Nishina cross section that impact the sampling methods. The relationship between the forward and adjoint double differential cross section serves as a starting point in this discussion. The adjoint scattering energy range that can be extracted from this cross section relationship contains a discontinuity that must be characterized and avoided before sampling methods can be constructed. In section III, the sampling methods for the adjoint Klein-Nishina cross section will be developed and discussed. Section IV examines the sampling efficiencies and speeds of the methods. Finally in section V, the results of an infinite medium problem generated using the Framework for REsearch in Nuclear ScIence and Engineering (FRENSIE) [4, 5, 6], in which the new sampling methods have been implemented, are presented.

II. THE ADJOINT KLEIN-NISHINA CROSS SECTION

The following relationship between the forward and the adjoint cross section can be used to construct the adjoint Klein-Nishina cross section from the Klein-Nishina cross section:

$$\frac{d^2\sigma^{\dagger}_{KN}(E^{'}, E, \theta)}{d\Omega dE} = \frac{d^2\sigma_{KN}(E, E^{'}, \theta)}{d\Omega^{'} dE^{'}}. \tag{1}$$

This relationship can be constructed from a derivation of the adjoint transport equation [7]. It indicates that the adjoint cross section can be constructed from the forward cross section by swapping the variables that represent the incoming and outgoing quantities. For the remainder of this

work, primed variables will be used to refer to quantities before the collision, while unprimed variables will be used to refer to quantities after the collision. This convention will apply to both forward and adjoint cross sections. It must also be noted that the exact relationship between an adjoint cross section and a forward cross section includes incoming and outgoing directions. However, the Klein-Nishina cross section only depends on the cosine of the angle between the incoming and outgoing directions, which will not change if incoming and outgoing direction variables are swapped.

The Klein-Nishina cross section has the following form when photons have no net polarization [8]:

$$\frac{d^2\sigma_{KN}(E^{'},E,\theta)}{d\Omega dE} = \frac{r_e^2}{2}\left(\frac{\alpha}{\alpha^{'}}\right)^2\left[\frac{\alpha}{\alpha^{'}}+\frac{\alpha^{'}}{\alpha}-1+\left(\hat{\Omega}\cdot\hat{\Omega}^{'}\right)^2\right]\delta\left(E-\frac{E^{'}}{1+\alpha^{'}(1-\hat{\Omega}\cdot\hat{\Omega}^{'})}\right). \tag{2}$$

Note that in the above equation the scattering angle cosine has been represented as the dot product of the incoming and outgoing directions. Several of the energy variables have also been replaced with α variables. Each α variable is simply the ratio of the corresponding energy variable and the electron rest mass energy. Finally, the value r_e is the classical radius of the electron.

The delta function in equation 2 indicates that there is a one-to-one correspondence between the outgoing photon energy and scattering angle cosine. The outgoing photon energy from a Compton scattering event with a free electron can be determined using conservation of energy and momentum:

$$E = \frac{E^{'}}{1+\alpha^{'}(1-\cos\theta)}. \tag{3}$$

The double differential adjoint Klein-Nishina cross section can be constructed from equations 1 and 2 and is

$$\frac{d^2\sigma^{\dagger}_{KN}(E^{'},E,\theta)}{d\Omega dE} = \frac{r_e^2}{2}\left(\frac{\alpha^{'}}{\alpha}\right)^2\left[\frac{\alpha^{'}}{\alpha}+\frac{\alpha}{\alpha^{'}}-1+\left(\hat{\Omega}^{'}\cdot\hat{\Omega}\right)^2\right]\delta\left(E^{'}-\frac{E}{1+\alpha(1-\hat{\Omega}^{'}\cdot\hat{\Omega})}\right). \tag{4}$$

Before this equation can be used, the delta function must be modified so that the outgoing energy is once again the independent variable. The following delta function identity can be used to modify the delta function:

$$\delta(cx) = \frac{1}{|c|}\delta(x).$$

After using the delta function identity and completing some algebraic manipulations, one obtains the following for the delta function found in equation 4:

$$\delta\left(E^{'} - \frac{E}{1+\alpha(1-\cos\theta)}\right) = \left(\frac{\alpha}{\alpha^{'}}\right)^{2} \delta\left(E - \frac{E^{'}}{1-\alpha^{'}(1-\cos\theta)}\right) \tag{5}$$

Note that during the modification of the delta function the relationship between the outgoing adjoint photon energy and the scattering angle cosine is also derived:

$$E = \frac{E^{'}}{1-\alpha^{'}(1-\cos\theta)}. \tag{6}$$

This equation can also be found by solving equation 3 for the incoming energy and swapping primed and unprimed variables. Equation 6 will be discussed more shortly.

Using the delta function relationship from equation 5, a usable form of the double differential adjoint Klein-Nishina cross section is created:

$$\frac{d^{2}\sigma^{\dagger}_{KN}(E^{'},E,\theta)}{d\Omega dE} = \frac{r_{e}^{2}}{2}\left[\frac{\alpha^{'}}{\alpha} + \frac{\alpha}{\alpha^{'}} - 1 + \cos^{2}\theta\right]\delta\left(E - \frac{E^{'}}{1-\alpha^{'}(1-\cos\theta)}\right). \tag{7}$$

Integrating over all outgoing energies will then yield the differential adjoint Klein-Nishina cross section, where the one-to-one correspondence between the outgoing energy and the outgoing scattering angle is implicit:

$$\frac{d\sigma^{\dagger}_{KN}(E^{'},\theta)}{d\Omega} = \frac{r_{e}^{2}}{2}\left[\frac{\alpha^{'}}{\alpha} + \frac{\alpha}{\alpha^{'}} - 1 + \cos^{2}\theta\right]. \tag{8}$$

Before methods for sampling an outgoing energy and scattering angle cosine can be created, some observations regarding the relationship between the outgoing adjoint photon energy and the scattering angle cosine, characterized by equation 6, are discussed. A similar analysis can be found in work by Hoogenboom and Gabler et al [7, 1]. First, this equation exhibits a discontinuity when

$$\cos\theta = 1 - \frac{1}{\alpha^{'}}.$$

Any value of $\cos\theta$ less than the above value will result in nonphysical (negative) energies. Acceptable values of $\cos\theta$ that approach the above value will result in very large outgoing adjoint

photon energies. Because of the discontinuity in equation 6, it is more useful to characterize the bounds of a single adjoint Compton scattering event using the range of possible scattering angles instead of the range of possible outgoing energies, as is typically done with Compton scattering. The minimum scattering angle cosine is

$$\cos\theta_{min} = \begin{cases} -1 & \text{if } \alpha^{'} < \frac{1}{2} \\ 1 - \frac{1}{\alpha^{'}} & \text{if } \alpha^{'} \geq \frac{1}{2}. \end{cases} \tag{9}$$

The maximum scattering angle cosine is one, as it is with Compton scattering.

Second, this discontinuity introduces a singularity into the differential adjoint Klein-Nishina cross section that is not integrable. As will be shown shortly, the creation of a PDF from equation 8 requires, in theory, the integrated adjoint Klein-Nishina cross section. To avoid this singularity in the integration of the differential adjoint Klein-Nishina cross section a new parameter is introduced: the maximum problem energy, E_{max} [7]. As every physical model will have a maximum source energy, this new parameter is an acceptable requirement. Associated with this maximum energy will be a new minimum scattering angle cosine:

$$\begin{aligned} E_{max} &= \frac{E^{'}}{1 - \alpha^{'}(1 - \cos\theta_{min})}, \\ \cos\theta_{min} &= \begin{cases} -1 & \text{if } \alpha^{'} < \frac{\alpha_{max}}{1+2\alpha_{max}} \\ 1 - \frac{1}{\alpha^{'}} + \frac{1}{\alpha_{max}} & \text{if } \alpha^{'} \geq \frac{\alpha_{max}}{1+2\alpha_{max}}. \end{cases} \end{aligned} \tag{10}$$

With these characteristics of the adjoint Klein-Nishina cross section in mind, sampling procedures are constructed. All of the sampling methods that are discussed in the following section have been implemented in the Framework for REsearch in Nuclear ScIence and Engineering (FRENSIE) [4, 5, 6].

III. SAMPLING METHODS

In this section adjoint Klein-Nishina sampling methods that have been developed will be discussed. It will first be shown that a form of direct sampling from the adjoint Klein-Nishina cross section, which is analogous to a form commonly employed with the Klein-Nishina cross

section, is not possible at any energy. A brief derivation and construction of the rejection sampling methods will then be provided.

III.A. Direct Sampling

To begin, the differential adjoint Klein-Nishina cross section will be converted to a variable that expresses both of the outgoing parameters simultaneously, which is analogous to what is done with Kahn's and Koblinger's differential Klein-Nishina cross section sampling methods [9, 10, 11]. The inverse energy gain ratio, $x^{\dagger}$, is one such parameter that can be used for this purpose:

$$x^{\dagger} = \frac{\alpha^{'}}{\alpha} = 1 - \alpha^{'}(1 - \cos\theta). \tag{11}$$

After conducting the change of variable, the double differential adjoint Klein-Nishina cross section becomes the following:

$$\frac{d^2\sigma^{\dagger}_{KN}(E^{'}, x^{\dagger})}{dx^{\dagger}} = K^{\dagger}\left[A^{\dagger}x^{\dagger 2} + B^{\dagger}x^{\dagger} + C^{\dagger} + \frac{1}{x^{\dagger}}\right], \tag{12}$$

$$\text{where} \quad K^{\dagger} = \frac{\pi r_e^2}{\alpha^{'}}, \quad A^{\dagger} = \frac{1}{\alpha^{'2}}, \quad B^{\dagger} = 1 + \frac{2(\alpha^{'} - 1)}{\alpha^{'2}} \quad \text{and} \quad C^{\dagger} = \frac{1 - 2\alpha^{'}}{\alpha^{'2}}.$$

Now, a PDF for $x^{\dagger}$ can be created if the double differential adjoint Klein-Nishina cross section is divided by the integrated adjoint Klein-Nishina cross section. The integrated adjoint Klein-Nishina cross section can be found by integrating the double differential adjoint Klein-Nishina cross section shown in equation 12 from $x^{\dagger}_{min}$ to $x^{\dagger}_{max} = 1$. Like the minimum scattering angle cosine, the minimum inverse energy gain ratio is a function of the max problem energy to avoid the aforementioned singularity:

$$x^{\dagger}_{min} = \begin{cases} 1 - 2\alpha^{'} & \text{if } \alpha^{'} < \frac{\alpha_{max}}{1+2\alpha_{max}} \\ \frac{\alpha^{'}}{\alpha_{max}} & \text{if } \alpha^{'} \geq \frac{\alpha_{max}}{1+2\alpha_{max}}. \end{cases} \tag{13}$$

The integration of the adjoint Klein-Nishina is quite complex, and since in practice it will not be required for the sampling routine, there is no need to evaluate it.

The PDF for $x^\dagger$ can be defined as

$$p^\dagger_{KN}(E^{'}, E_{max}, x^\dagger) = \begin{cases} H^\dagger \left[A^\dagger x^{\dagger 2} + B^\dagger x^\dagger + C^\dagger + \frac{1}{x^\dagger}\right] & \text{if } x^\dagger_{min} \leq x^\dagger \leq 1 \\ 0 & \text{otherwise,} \end{cases} \tag{14}$$

$$\text{where} \quad H^\dagger = \frac{K^\dagger}{\sigma^\dagger_{KN}(E', E_{max})}.$$

Unfortunately, there is no range of energies where all of the terms of this PDF are simultaneously positive (the $B^\dagger$ and $C^\dagger$ terms impose conflicting constraints), which means that it is not possible to construct a direct sampling method analogous to Koblinger's sampling method [11].

III.B. Rejection Sampling

As was done by Kahn with the differential Klein-Nishina cross section, the differential adjoint Klein-Nishina cross section shown in equation 12 can be reorganized so that none of the terms are negative at any energy [10]. The resulting PDF for the inverse energy gain ratio is the following:

$$p^\dagger_{KN}(E^{'}, E_{max}, x^\dagger) = \begin{cases} H^\dagger \left[\left(\frac{1}{x^\dagger} - 1\right) + x^\dagger + cos^2\theta\right] & \text{if } x^\dagger_{min} \leq x^\dagger \leq 1 \\ 0 & \text{otherwise.} \end{cases} \tag{15}$$

Rejection sampling procedures can be constructed by splitting this PDF into either two terms or three terms and there are merits to both approaches, as will be explained in the next section.

The specific rejection method considered for sampling from the adjoint Klein-Nishina cross section assumes that the PDF of interest can be factored into several terms. The PDF is factored into the following form, where m is the number of terms, p_i is the probability of selecting term i, $T_i(z)$ is the rejection function for term i, $n_i(z)$ is a PDF used to sample a z value from term i and κ is the theoretical efficiency of the sampling procedure [12]:

$$p(z) = \sum_i^m f_i(z) = \frac{\sum_i^m p_i T_i(z) n_i(z)}{\kappa}. \tag{16}$$

The number of terms, m, is arbitrary although splitting a PDF into more terms can often improve the sampling efficiency since each term can more accurately represent a part of the PDF [10]. It must be noted that each p_i term must be in the interval [0,1] and that they must sum to one -

i.e. they form a discrete distribution. The $n_i(z)$ PDFs can take any form that is desired. It must be noted that Kahn's Klein-Nishina rejection sampling procedure is an example of this technique [10].

When carrying out this factorization into m terms, the following system of $m+1$ equations and $m+1$ unknowns can be constructed to solve for the p_i and κ terms once the $T_i(z)$ and $n_i(z)$ functions have been chosen:

$$\frac{p_i}{\kappa} = \frac{f_i(z)}{T_i(z)n_i(z)}, \tag{17}$$

$$\sum_i^m p_i = 1. \tag{18}$$

This system of equations can be simplified by introducing a constant of proportionality, C_i, for each term:

$$C_i T_i(z) n_i(z) = f_i(z)$$

$$C_i = \frac{f_i(z)}{T_i(z)n_i(z)} = \frac{p_i}{\kappa}. \tag{19}$$

Using the last line of the system of equations, the κ term can be solved for:

$$\kappa = \left(\sum_{i=0}^{m} C_i \right)^{-1}. \tag{20}$$

Finally, by using equation 17 and equation 19, the p_i terms can be determined:

$$p_i = \kappa C_i = \frac{C_i}{\sum_{i=0}^{m} C_i}. \tag{21}$$

With the system of equations solved, the sampling technique is now completely defined.

To use this generalized rejection sampling technique, one must first sample a term i using the p_i terms. Since the p_i terms form a discrete distribution, the term i can be sampled using a

single uniform random number ε_1 from the interval [0,1):

$$i = \begin{cases} 1 & \text{if } \varepsilon_1 \leq p_1 \\ 2 & \text{if } p_1 < \varepsilon_1 \leq p_1 + p_2 \\ & ... \\ m-1 & \text{if } \sum_1^{m-2} p_i < \varepsilon_1 \leq \sum_1^{m-1} p_i \\ m & \text{otherwise.} \end{cases} \tag{22}$$

Once a term i has been sampled, a value of z is sampled from the PDF $n_i(z)$ using another uniform random number ε_2 from the interval [0,1). Finally the sampled value of z is accepted if the following equality holds, where ε_3 is another uniform random number from the interval [0,1):

$$\varepsilon_3 \leq T_i(z).$$

If the value of z is rejected the entire sampling process must be restarted with the sampling of a new term i.

III.B.1. Two-Branch Rejection Sampling

The first sampling procedure that will be developed is purposefully simple and serves as the baseline for the speed and efficiency comparisons. As will be shown in the next section, despite this method's relatively low efficiency, its simplicity actually results in it having a superior sampling speed in certain situations.

To derive this procedure, the PDF shown in equation 15 will be split into two terms and expressed in a way that is similar to equation 16:

$$\begin{aligned} \kappa p^{\dagger}_{KN}(E', E_{max}, x^{\dagger}) = {} & p_1(E', E_{max}) T_1(E', E_{max}, x^{\dagger}) n_1(E', E_{max}, x^{\dagger}) + \\ & p_2(E', E_{max}) T_2(E', E_{max}, x^{\dagger}) n_2(E', E_{max}, x^{\dagger}). \end{aligned}$$

The constants of proportionality are the following:

$$C_1(E^{'}, E_{max}) = H^{\dagger}\left(\frac{1}{x^{\dagger}} - 1\right)\frac{1}{T_1(E^{'}, E_{max}, x^{\dagger})n_1(E^{'}, E_{max}, x^{\dagger})}, \tag{23}$$

$$C_2(E^{'}, E_{max}) = H^{\dagger}\left(x^{\dagger} + \cos^2\theta\right)\frac{1}{T_2(E^{'}, E_{max}, x^{\dagger})n_2(E^{'}, E_{max}, x^{\dagger})} \tag{24}$$

For the first term, the simplest way to generate a sample is by first sampling $x^{\dagger}$ from the uniform distribution:

$$n_1(E^{'}, E_{max}, x^{\dagger}) = \frac{1}{1 - x^{\dagger}_{min}}. \tag{25}$$

The rejection function for the first term must then be the following:

$$T_1(E^{'}, E_{max}, x^{\dagger}) = \frac{x^{\dagger}_{min}}{1 - x^{\dagger}_{min}}\left(\frac{1}{x^{\dagger}} - 1\right). \tag{26}$$

Note that the maximum value of this rejection function occurs when $x^{\dagger} = x^{\dagger}_{min}$. With n_1 and T_1 determined, the constant of proportionality C_1 can now be calculated:

$$C_1(E^{'}, E_{max}) = \frac{H^{\dagger}\left(1 - x^{\dagger}_{min}\right)^2}{x^{\dagger}_{min}}. \tag{27}$$

For the second term, the simplest way to generate a sample is by first sampling $x^{\dagger}$ from a uniform distribution:

$$n_2(E^{'}, E_{max}, x^{\dagger}) = \frac{1}{1 - x^{\dagger}_{min}}. \tag{28}$$

The rejection function for the second term must then be

$$T_2(E^{'}, E_{max}, x^{\dagger}) = \frac{1}{2}\left[x^{\dagger} + \left(1 - \frac{(1 - x^{\dagger})}{\alpha^{'}}\right)^2\right]. \tag{29}$$

Note that the maximum value of this function occurs when $x^{\dagger}$ equals one and correspondingly, the scattering angle cosine equals one. The resulting constant of proportionality C_2 is the following:

$$C_2(E^{'}, E_{max}) = 2H^{\dagger}\left(1 - x^{\dagger}_{min}\right). \tag{30}$$

With the constants of proportionality calculated the theoretical sampling efficiency can be

determined:

$$\kappa = \frac{x^{\dagger}_{min}}{H^{\dagger}\left(1 - x^{\dagger}_{min}\right)\left(1 + x^{\dagger}_{min}\right)}. \tag{31}$$

Finally, the p_i terms can be calculated:

$$p_1(E^{'}, E_{max}) = \frac{1 - x^{\dagger}_{min}}{1 + x^{\dagger}_{min}}, \tag{32}$$

$$p_2(E^{'}, E_{max}) = \frac{2x^{\dagger}_{min}}{1 + x^{\dagger}_{min}}. \tag{33}$$

This rejection sampling procedure, which will be referred to as the *two-branch rejection sampling procedure*, is shown in figure 1.

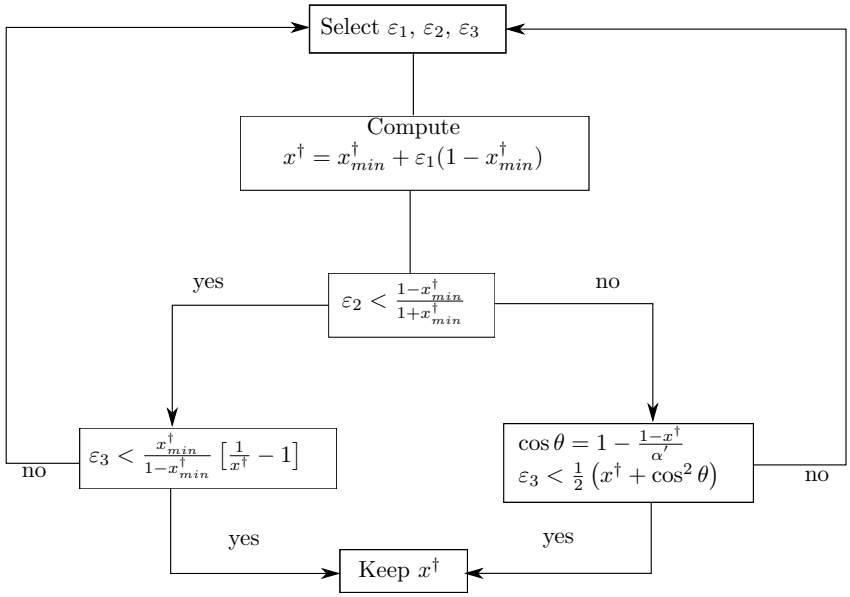

Fig. 1. **The two-branch adjoint Klein-Nishina rejection sampling procedure**. *This sampling procedure is used to sample a value of $x^{\dagger}$ from the differential adjoint Klein-Nishina cross section. ε_1, ε_2 and ε_3 are uniform random numbers from the interval [0,1).*

III.B.2. Three-Branch Sampling Methods

The remaining two sampling procedures that will be developed prioritize sampling efficiency over evaluation simplicity. These procedures can be created by splitting the PDF shown in equation

15 into three terms:

$$\begin{aligned}\kappa p^{\dagger}_{KN}(E^{'}, E_{max}, x^{\dagger}) = p_1(E^{'}, E_{max}) T_1(E^{'}, E_{max}, x^{\dagger}) n_1(E^{'}, E_{max}, x^{\dagger}) + \\ p_2(E^{'}, E_{max}) T_2(E^{'}, E_{max}, x^{\dagger}) n_2(E^{'}, E_{max}, x^{\dagger}) + \\ p_3(E^{'}, E_{max}) T_3(E^{'}, E_{max}, x^{\dagger}) n_3(E^{'}, E_{max}, x^{\dagger}).\end{aligned}$$

The constants of proportionality are the following:

$$C_1(E^{'}, E_{max}, x^{\dagger}) = H^{\dagger}\left(\frac{1}{x^{\dagger}} - 1\right) \frac{1}{T_1(E', E_{max}, x^{\dagger}) n_1(E', E_{max}, x^{\dagger})}, \tag{34}$$

$$C_2(E^{'}, E_{max}, x^{\dagger}) = H^{\dagger}\left(x^{\dagger}\right) \frac{1}{T_2(E', E_{max}, x^{\dagger}) n_2(E', E_{max}, x^{\dagger})}, \tag{35}$$

$$C_3(E^{'}, E_{max}, x^{\dagger}) = H^{\dagger}\left(\cos^2\theta\right) \frac{1}{T_3(E', E_{max}, x^{\dagger}) n_3(E', E_{max}, x^{\dagger})}. \tag{36}$$

For the first term, there are two ways that one can efficiently sample a value of $x^{\dagger}$:

$$n_{1,lin}(E^{'}, E_{max}, x^{\dagger}) = \frac{2(1 - x^{\dagger})}{\left(1 - x^{\dagger}_{min}\right)^2}, \tag{37}$$

$$n_{1,inv}(E^{'}, E_{max}, x^{\dagger}) = \frac{-1}{x \ln(x^{\dagger}_{min})}. \tag{38}$$

The first PDF is a linear distribution and the second PDF is an inverse distribution, hence the *lin* and *inv* subscripts respectively. The corresponding rejection functions for the first term are the following:

$$T_{1,lin}(E^{'}, E_{max}, x^{\dagger}) = \frac{x^{\dagger}_{min}}{x^{\dagger}}, \tag{39}$$

$$T_{1,inv}(E^{'}, E_{max}, x^{\dagger}) = \frac{1 - x^{\dagger}}{1 - x^{\dagger}_{min}}. \tag{40}$$

For both variations of the rejection function, the maximum value occurs when $x^{\dagger}$ equals its minimum value. With both forms of $n_1(E^{'}, E_{max}, x^{\dagger})$ and $T_1(E^{'}, E_{max}, x^{\dagger})$ determined, the two con-

stants of proportionality can now be calculated:

$$C_{1,lin}(E^{'}, E_{max}) = \frac{H^{\dagger}\left(1 - x_{min}^{\dagger}\right)^{2}}{2x_{min}^{\dagger}}, \tag{41}$$

$$C_{1,inv}(E^{'}, E_{max}) = -H^{\dagger}(1 - x_{min}^{\dagger}) \ln x_{min}^{\dagger}. \tag{42}$$

For the second and third terms, a direct sampling method can be constructed from the following PDFs:

$$n_2(E^{'}, E_{max}, x^{\dagger}) = \frac{2x^{\dagger}}{1 - x_{min}^{\dagger 2}}, \tag{43}$$

$$n_3(E^{'}, E_{max}, x^{\dagger}) = \frac{3(x^{\dagger} - 1 + \alpha^{'})^2}{\alpha^{'3} - (x_{min}^{\dagger} - 1 + \alpha^{'})^3}. \tag{44}$$

Given that $x^{\dagger}$ values can be sampled directly for the second and third terms, there are no rejection functions associated with those terms. The constants of proportionality $C_2(E^{'}, E_{max})$ and $C_3(E^{'}, E_{max})$ can now be calculated:

$$C_2(E^{'}, E_{max}) = \frac{1}{2} H^{\dagger}\left(1 - x_{min}^{\dagger 2}\right), \tag{45}$$

$$C_3(E^{'}, E_{max}) = H^{\dagger}\left[\frac{\alpha^{'3} - \left(x_{min}^{\dagger} - 1 + \alpha^{'}\right)^3}{3\alpha^{'2}}\right]. \tag{46}$$

Before the two variations of the sampling procedure can be completed the selection probabilities must be calculated. The selection probabilities associated with the *lin* variation is calculated first. The theoretical efficiency associated with the *lin* variation is the following:

$$\frac{1}{\kappa_{lin}}\left(\frac{2x_{min}^{\dagger}}{H^{\dagger}}\right) = \left[\left(1 - x_{min}^{\dagger}\right)^2 + x_{min}^{\dagger}\left(1 - x_{min}^{\dagger 2}\right)\right] + \left(\frac{2x_{min}^{\dagger}}{3\alpha^{'2}}\right)\left[\alpha^{'3} - \left(x_{min}^{\dagger} - 1 + \alpha^{'}\right)^3\right]. \tag{47}$$

The $p_{i,lin}$ terms are therefore

$$p_{1,lin}(E^{'}, E_{max}) = \left(1 - x^{\dagger}_{min}\right)^2 / \left[\frac{1}{\kappa_{lin}}\left(\frac{2x^{\dagger}_{min}}{H^{\dagger}}\right)\right], \tag{48}$$

$$p_{2,lin}(E^{'}, E_{max}) = x^{\dagger}_{min}\left(1 - x^{\dagger 2}_{min}\right) / \left[\frac{1}{\kappa_{lin}}\left(\frac{2x^{\dagger}_{min}}{H^{\dagger}}\right)\right], \tag{49}$$

$$p_{3,lin}(E^{'}, E_{max}) = \left(\frac{2x^{\dagger}_{min}}{3\alpha^{'}}\right)\left[\alpha^{'3} - \left(x^{\dagger}_{min} - 1 + \alpha^{'}\right)^3\right] / \left[\frac{1}{\kappa_{lin}}\left(\frac{2x^{\dagger}_{min}}{H^{\dagger}}\right)\right]. \tag{50}$$

This rejection sampling procedure will be referred to as the *three-branch linear rejection sampling procedure* and is shown in figure 2.

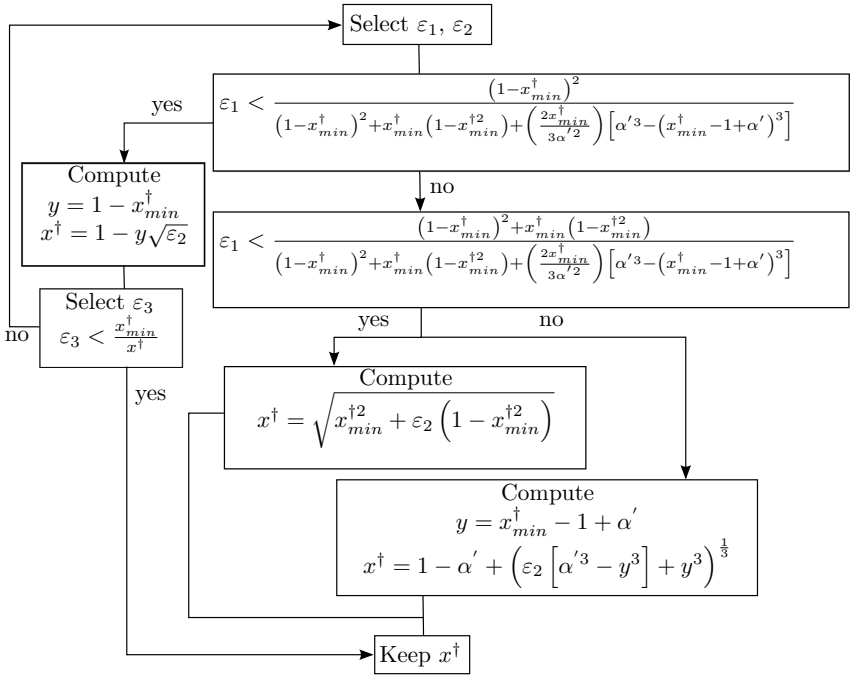

Fig. 2. **The three-branch linear adjoint Klein-Nishina rejection sampling procedure**. *This sampling procedure is used to sample a value of $x^{\dagger}$ from the differential adjoint Klein-Nishina cross section. ε_1, ε_2 and ε_3 are uniform random numbers from the interval [0,1).*

The selection probabilities associated with the *inv* variation of the three-branch sampling procedure will now be calculated. The theoretical efficiency associated with the *inv* variation is

the following:

$$\frac{1}{\kappa_{inv}}\left(\frac{3\alpha^{'2}}{H^{\dagger}}\right)=\left[-3(1-x^{\dagger}_{min})\ln x^{\dagger}_{min}\alpha^{'2}+\frac{3}{2}\left(1-x^{\dagger 2}_{min}\right)\alpha^{'2}\right]+\left[\alpha^{'3}-\left(x^{\dagger}_{min}-1+\alpha^{'}\right)^{3}\right]. \tag{51}$$

The $p_{i,inv}$ terms are therefore

$$p_{1,inv}(E^{'},E_{max})=-3\ln x^{\dagger}_{min}(1-x^{\dagger}_{min})\alpha^{'2}/\left[\frac{1}{\kappa_{inv}}\left(\frac{3\alpha^{'2}}{H^{\dagger}}\right)\right], \tag{52}$$

$$p_{2,inv}(E^{'},E_{max})=\frac{3}{2}\left(1-x^{\dagger 2}_{min}\right)\alpha^{'2}/\left[\frac{1}{\kappa_{inv}}\left(\frac{3\alpha^{'2}}{H^{\dagger}}\right)\right], \tag{53}$$

$$p_{3,inv}(E^{'},E_{max})=\alpha^{'3}-\left(x^{\dagger}_{min}-1+\alpha^{'}\right)^{3}/\left[\frac{1}{\kappa_{inv}}\left(\frac{3\alpha^{'2}}{H^{\dagger}}\right)\right]. \tag{54}$$

This rejection sampling procedure will be referred to as the *three-branch inverse rejection sampling procedure* and is shown in figure 3.

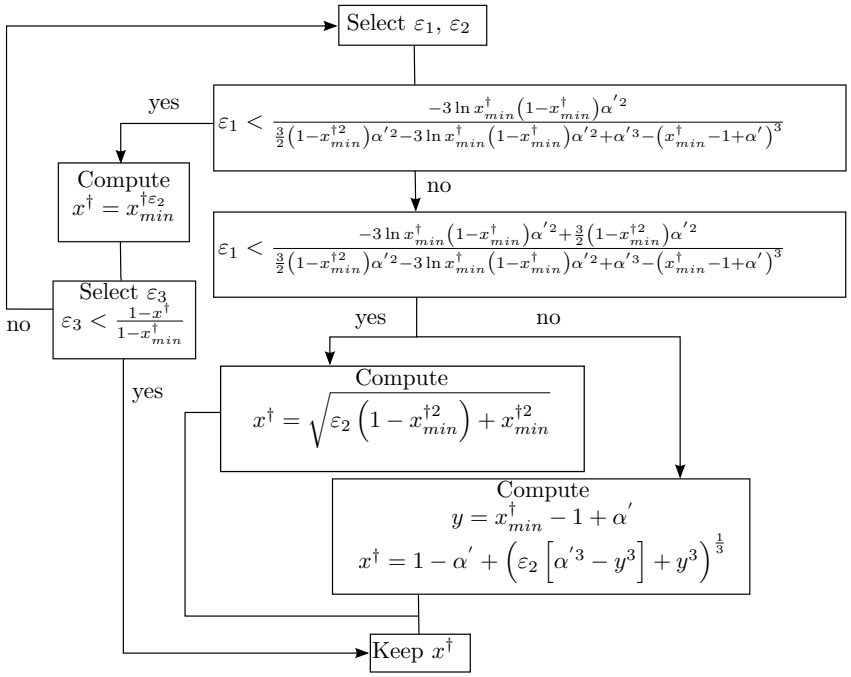

Fig. 3. **The three-branch inverse adjoint Klein-Nishina rejection sampling procedure**. *This sampling procedure is used to sample a value of $x^{\dagger}$ from the differential adjoint Klein-Nishina cross section. ε_1, ε_2 and ε_3 are uniform random numbers from the interval [0,1).*

IV. SAMPLING EFFICIENCIES AND SPEEDS

To determine which sampling method should be used the sampling efficiency of each method must be evaluated at a range of incoming adjoint photon energies and max problem energies. Due to the large number of special functions and some non-integer exponents that appear in the *three-branch inverse rejection sampling procedure*, which can be costly to evaluate, the sample generation rate must also be evaluated. These data are shown in figure 4. The relative sample rate data shown in this figure are noisy, which may be due to the granularity of system timing routines and the resulting difficulties of using them for timing short segments of code. To aide in visualizing the trends in the relative sample rate data, curve fits generated using a finite impulse response filter are also plotted [13].

Based on figure 4 it is clear that, while the *three-branch linear rejection sampling method* does not always have the highest efficiency at all energies, it usually has the highest sample generation rate. Interestingly, the *two-branch linear rejection sampling method* often has a comparable sample rate to the *three-branch inverse rejection sampling method* despite its significantly lower efficiency. This rather unexpected result highlights the need to balance evaluation simplicity and sampling efficiency.

Because there are energy ranges where each procedure outperforms the other two, there is likely a more efficient, combined procedure that could be created that would utilize a given procedure when optimal. This would likely require the development of tables that describe which procedure to use at a given energy and max problem energy. Analyzing the theoretical efficiencies to see where those functions cross for arbitrary energies and max problem energies could be useful in the development of those tables.

IV.A. Bound Electron Effects

In most realistic simulations, the electrons are assumed to be bound. The primary way the bound electron effects are accounted for with regards to the outgoing photon direction is through the scattering function [14]. The scattering function is simply a correction factor that multiplies the Klein-Nishina cross section, as shown in the following equation:

$$\frac{d\sigma_{inc}(E^{'},\theta,Z)}{d\Omega} = \frac{d\sigma_{KN}(E^{'},\theta)}{d\Omega} S(E^{'},\theta,Z). \tag{55}$$

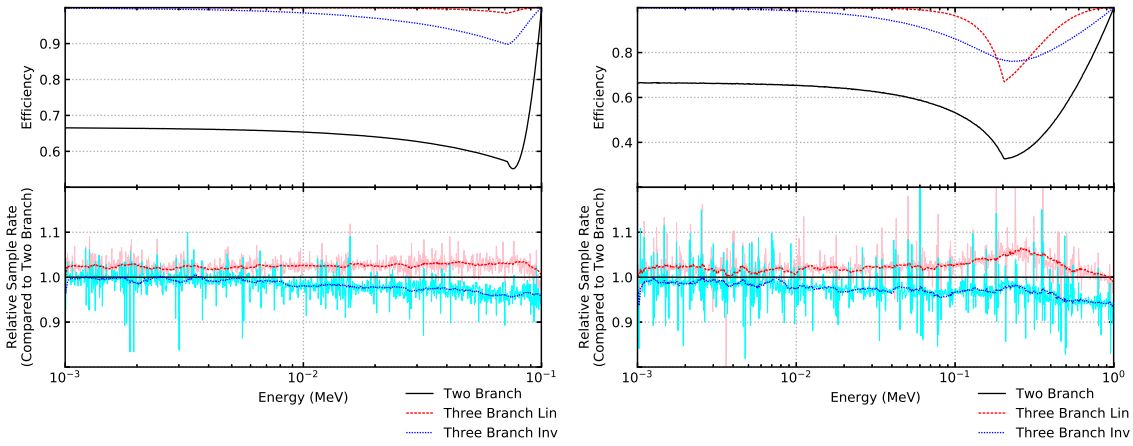

(a) $E_{max} = 100$ keV

(b) $E_{max} = 1$ MeV

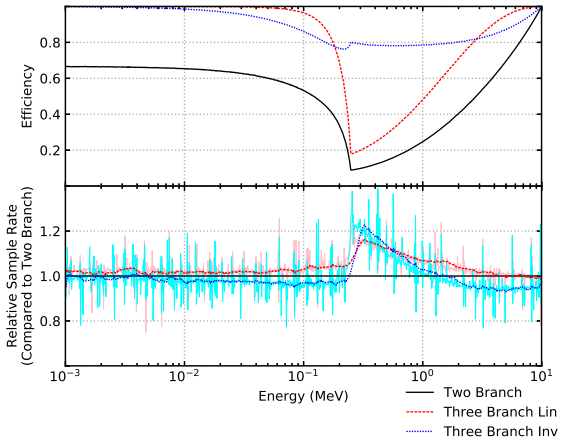

(c) $E_{max} = 10$ MeV

Fig. 4. **Differential adjoint Klein-Nishina cross section sampling procedure efficiencies and relative sample rates with a max energy 100 keV (a), 1 MeV (b) and 10 MeV (c).** *To generate the efficiency and sample rate data,* 10^5 *samples were generated three separate times at each adjoint photon energy (about 1000 equally spaced energies on a log scale were chosen). The average of the efficiency and the relative sample rate over the three trials are presented in this figure. Because the relative sample rate data are noisy, curve fits are also provided to help visualize trends.*

The scattering function ranges from a value of zero to Z, the atomic number of the atom that the electrons are bound within. The resulting cross section is usually referred to as the incoherent scattering cross section. The incorporation of this scattering function into the cross section has the potential to decrease the sampling efficiency compared to the free electron case [15]. The particular way that the sampling efficiency is negatively affected by the scattering function is important to analyze when choosing a sampling method.

The construction of an equivalent adjoint incoherent cross section will use the same steps that were outlined in section II for the construction of the adjoint Klein-Nishina cross section. The resulting adjoint incoherent scattering cross section is the following:

$$\frac{d\sigma^{\dagger}_{inc}(E^{'},\theta,Z)}{d\Omega} = \frac{d\sigma^{\dagger}_{KN}(E^{'},\theta)}{d\Omega} S(E,\theta,Z). \tag{56}$$

Note that in the adjoint incoherent scattering cross section the scattering function is evaluated at the outgoing energy and not the incoming energy. For simplicity, the scattering function evaluated at the outgoing energy will be referred to as the adjoint scattering function:

$$S^{\dagger}(E^{'},\theta,Z) = S\left(E(E^{'},\theta),\theta,Z\right). \tag{57}$$

A sampling procedure for the outgoing photon energy and direction can be constructed by converting equation 56 into a PDF and reorganizing terms:

$$\begin{aligned} p^{\dagger}(E^{'},E_{max},\cos\theta,Z) &= \frac{1}{\sigma^{\dagger}_{inc}(E^{'},E_{max},Z)} \frac{d\sigma^{\dagger}_{inc}(E^{'},\theta,Z)}{d\Omega} \\ &= \frac{S^{\dagger}_{max}(E^{'},Z)\sigma^{\dagger}_{KN}(E^{'},E_{max})}{\sigma^{\dagger}_{inc}(E^{'},E_{max},Z)} \left[\frac{S^{\dagger}(E^{'},\theta,Z)}{S^{\dagger}_{max}(E^{'},Z)}\right] \cdot \\ &\qquad \left[\frac{1}{\sigma^{\dagger}_{KN}(E^{'},E_{max})} \frac{d\sigma^{\dagger}_{KN}(E^{'},\theta)}{d\Omega}\right] \\ &= \frac{1}{\kappa_{inc}(E^{'},E_{max},Z)} R^{\dagger}(E^{'},E_{max},\theta,Z) p^{\dagger}_{KN}(E^{'},E_{max},\cos\theta). \end{aligned} \tag{58}$$

To use this sampling method, one must first sample an outgoing scattering angle cosine from the adjoint Klein-Nishina PDF, $p^{\dagger}_{KN}(E^{'},E_{max},\cos\theta)$, using one of the procedures discussed in the previous section. Once the scattering angle cosine has been sampled, the following rejection

function must be evaluated to determine if the scattering angle cosine should be rejected:

$$R^{\dagger}(E^{'}, E_{max}, \theta, Z) = \frac{S^{\dagger}\left(E^{'}, \theta, Z\right)}{S^{\dagger}_{max}\left(E^{'}, Z\right)} = \frac{S^{\dagger}\left(E^{'}, \theta, Z\right)}{S^{\dagger}\left(E^{'}, \theta_{min}, Z\right)}. \tag{59}$$

The κ_{inc} term represents the theoretical sampling efficiency of this rejection function. This method is analogous to the method developed by Persliden for incoherent scattering [15].

Figure 5 shows the efficiency of the overall sampling procedure, using the *three-branch linear rejection sampling procedure* to sample from the adjoint Klein-Nishina cross section, for max problem energies of 100 keV, 1 MeV and 10 MeV and for a free electron, aluminum and lead. For lower energies, energies very close to the max problem energy and higher atomic numbers, the adjoint scattering function causes a large decrease in the efficiency of the sampling procedure compared to the free electron case. Fortunately, the adjoint Klein-Nishina rejection sampling methods that have been developed perform best, in terms of efficiency, in the regions where the adjoint scattering function has the most deleterious affect on the sampling efficiency. This further indicates that the methods developed in the previous section are well suited to realistic simulations.

V. RESULTS

In the previous section, it was shown that the *three-branch linear rejection sampling procedure* can generate samples the fastest for most energies and max problem energies. To verify that this rejection sampling procedure is indeed suitable for use in a Monte Carlo simulation, the results of an infinite medium simulation generated using FRENSIE and this new adjoint Klein-Nishina rejection sampling procedure are examined. One advantage of this geometry, which is shown in figure 6, is that spherical and translational symmetries allow the adjoint simulation to be set up (nearly) identically to the forward simulation. Care must be taken when constructing the adjoint source energy distribution as it will differ from the forward source [17].

Photon flux results will be shown on the surface of a sphere of four centimeter radius centered on the source point. To be consistent with the efficiency and speed data that was discussed in the previous section, mono-energetic source energies of 100 keV and 1 MeV were considered. 10 MeV was not considered due to the importance of pair production at this energy, which is outside the scope of this discussion. For each simulation, 10^9 particle histories were simulated. The generation

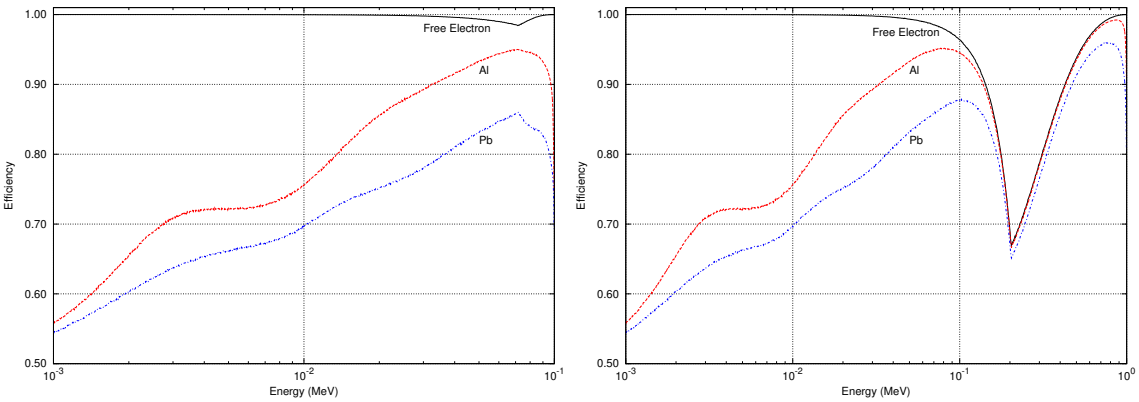

(a) $E_{max} = 100$ keV

(b) $E_{max} = 1$ MeV

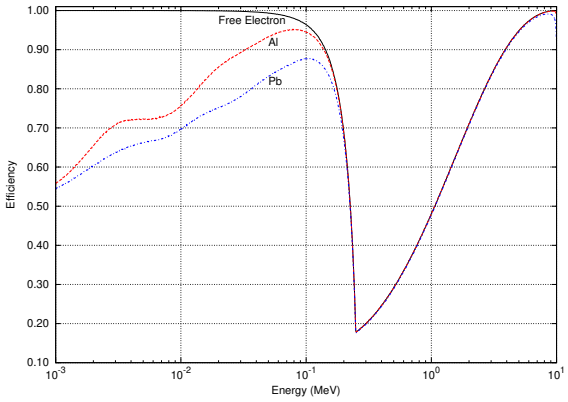

(c) $E_{max} = 10$ MeV

Fig. 5. **Differential adjoint incoherent cross section sampling procedure efficiencies for a max problem energy of 100 keV (a), 1 MeV (b) and 10 MeV (c).** *For every scattering center, the three-branch linear rejection sampling procedure was used to sample from the adjoint Klein-Nishina cross section. The Waller-Hartree scattering function was used in the rejection function of the incoherent scattering sampling procedure [16].*

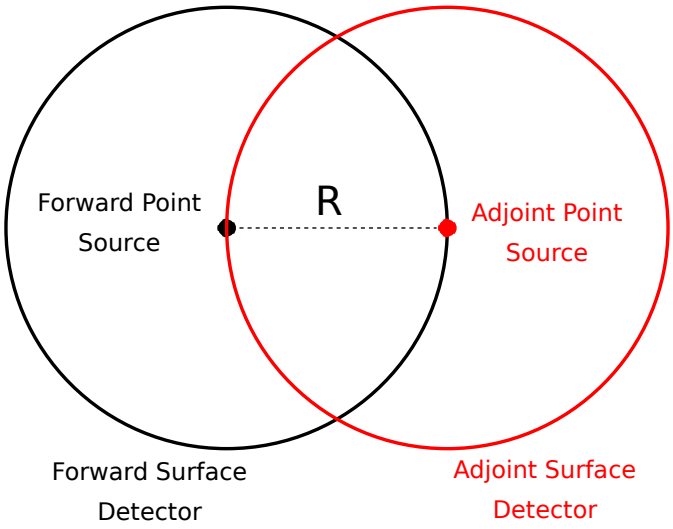

Fig. 6. **The infinite medium geometry and the symmetries used to construct a nearly identical adjoint simulation.** *A mono-energetic, isotropic point source is located at the center of a sphere with a 4 cm radius. The spatial domain extends to infinity in all directions. A surface flux estimator is placed on the spherical surface. Because the spatial domain is infinite, spherical and translational symmetries exist with respect to the point source. These symmetries allow the adjoint simulation to be set up in a nearly identical way to the forward simulation.*

of secondary particles and atomic relaxation were also disabled in these simulations.

Figure 7 shows the photon flux spectrum on the four centimeter spherical surface using a forward and adjoint simulation and the two source energies of interest. This figure also shows the ratio of the flux calculated using an adjoint simulation and a forward simulation, with the associated one sigma error bars (FA-WH/FF-WH) to facilitate comparisons between the spectra. At both source energies, the flux ratios indicate that there is good agreement between the adjoint simulation result and the forward simulation results.

The total photon flux on the four centimeter spherical surface using both simulation modes and both source energies is shown in table I. The forward and adjoint flux results are within two sigma at both source energies and the percent difference between the forward and adjoint results is no greater than 0.003%. Interestingly, the adjoint simulation takes between 2.31 and 3.67 times longer than the forward simulation. It is difficult to determine if this is due to the *three-branch linear rejection sampling procedure* or some other aspect of the adjoint simulation that differs from the forward simulation (e.g. the different source energy distribution or the required energy point detector to account for the discrete source energy [1]). A more detailed performance analysis of the adjoint simulation in FRENSIE will be done in the future to determine the cause of this

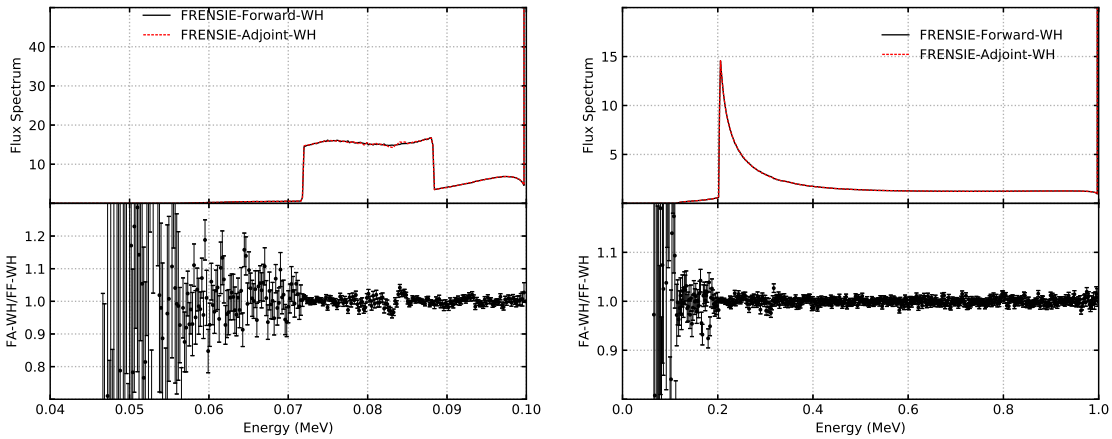

(a) $S_e = 100keV$ (b) $S_e = 1MeV$

Fig. 7. **Flux spectrum per source particle on the 4 cm radius sphere in an infinite lead medium resulting from a 100 keV source (a) and a 1 MeV source (b)** *The three-branch linear rejection sampling procedure was used in the adjoint simulations. All simulations accounted for binding effects of electrons using the Waller-Hartree scattering function for lead. The ratio of the flux calculated in FRENSIE using an adjoint simulation and a forward simulation is also shown in this plot. The good agreement between the forward and adjoint simulation flux results indicates that the three-branch linear rejection sampling procedure can indeed be successfully used in an adjoint simulation.*

performance difference.

TABLE I
Infinite Lead Medium Results

S_e (MeV)	Mode	Total Flux	Flux σ	% Diff.	Rel. Sim. Time
0.1	Forward	**4.704**00	0.00050	0.0	1.0
0.1	Adjoint	**4.704**13	0.00048	0.0028	3.67
1.0	Forward	**49.884**53	0.00049	0.0	1.0
1.0	Adjoint	**49.885**05	0.00039	0.0010	2.31

VI. CONCLUSION

Three new rejection sampling methods have been developed for generating samples from the adjoint Klein-Nishina cross section: the *two-branch rejection sampling procedure*, the *three-branch linear rejection sampling procedure* and the *three-branch inverse rejection sampling procedure*. Each of these methods have been implemented in FRENSIE. While there are energy ranges where each of these methods can generate samples faster than the others, the *three-branch linear rejection*

sampling procedure can consistently generate samples the fastest and is therefore recommended. The *three-branch inverse rejection sampling procedure* can consistently generate samples the most efficiently, but it is expensive to use and only outperforms the speed of the *three-branch linear rejection sampling procedure* in limited energy ranges. A combined method could be created that always uses the fastest method. However, given the complex nature of the adjoint Klein-Nishina cross section, this combined method will likely be difficult to construct for a general energy and max problem energy.

To verify that the recommended *three-branch linear rejection sampling procedure* can be used in a Monte Carlo simulation to generate samples from the adjoint Klein-Nishina cross section, the results of an infinite medium simulation generated using FRENSIE and this rejection sampling procedure were provided. The results of the adjoint simulations were shown to be in good agreement with the results of the forward simulations, which indicated that the *three-branch linear rejection sampling procedure* is indeed an effective sampling procedure for the adjoint Klein-Nishina cross section. Further performance analysis of the adjoint simulations must be done in FRENSIE to determine the cause of the longer adjoint simulation times compared to the forward simulations. It is not clear if the performance differences are due to the new adjoint Klein-Nishina sampling procedure or some other aspect of the adjoint simulation that differs from the forward simulation.

While these new methods allow one to efficiently and quickly generate samples from the adjoint Klein-Nishina cross section, even in realistic problems, there are likely better methods that could be discovered by completing a more detailed analysis of the adjoint Klein-Nishina cross section. The extremely thorough work by Mathews on the Klein-Nishina cross section could provide many valuable insights regarding ways to create new sampling methods for the adjoint Klein-Nishina cross section beyond the work that has been presented here [18].

ACKNOWLEDGMENTS

This work was partially supported by Nuclear Regulatory Commission Fellowship grants NRC-28-09-994 and NRC-38-10-954 and the Domestic Nuclear Detection Office: Academic Research Initiative grant 15DNARI0013-04-00. This work was also partially performed under the auspices of the U.S. Department of Energy by Lawrence Livermore National Laboratory under Contract DE-AC52-07NA27344.

This work describes objective technical results and analysis. Any subjective views or opinions that might've been expressed do not necessarily represent the views of the U.S. Department of Energy or the United States Government.

The authors would also like to thank Jürgen Henniger, Dorothea Gabler and Uwe Reichelt of the Technische Universität Dresden for their helpful discussions related to portions of this work and their generosity as hosts.

REFERENCES

[1] D. Gabler, J. Henniger, and U. Reichelt, "AMOS - An effective tool for adjoint Monte Carlo photon transport," *Nuclear Instruments and Methods in Physics Research Section B: Beam Interactions with Materials and Atoms*, **251**, *2*, 326 (2006).

[2] L. Desorgher, F. Lei, and G. Santin, "Implementation of the reverse/adjoint Monte Carlo method into Geant4," *Nuclear Instruments and Methods in Physics Research Section A: Accelerators, Spectrometers, Detectors and Associated Equipment*, **621**, *1-3*, 247 (2010).

[3] A. Robinson, B. Kiedrowski, and D. Henderson, "Status on the development of a Monte Carlo methods research framework," *ANS Meeting*, 111, Anaheim, CA, USA (2014).

[4] L. J. Kersting, D. Henderson, A. Robison, and E. Moll, "Energy deposition validation results for the evaluated electron data library in frensie," *20th Topical Meeting of the Radiation Protection & Shielding Division of ANS*, Santa Fe, NM, USA (2018).

[5] L. J. Kersting, D. Henderson, A. Robinson, and E. Moll, "Validation and verification of the evaluated electron data library in FRENSIE," *Nuclear Science and Engineering*, **193**, *4*, 346 (2019).

[6] L. J. Kersting, A. Robinson, E. Moll, P. Britt, L. Gross, and D. Henderson, "Single Scattering Adjoint Monte Carlo Electron Transport in FRENSIE," *Nuclear Science and Engineering*, **194**, *5*, 350 (2020).

[7] J. E. Hoogenboom, "Methodology of Continuous-Energy Adjoint Monte Carlo for Neutron, Photon, and Coupled Neutron-Photon Transport," *Nuclear Science and Engineering*, **143**, 99 (2003).

[8] Klein and Y. Nishina, "Uber die streuung von strahlung durch freie elektronen nach der neuen relativistischen quantendyamik," *Z. F. Phys.*, **52**, 853 (1929).

[9] I. Lux and L. Koblinger, *Monte Carlo Particle Transport Methods: Neutron and Photon Calculations*, CRC Press (1991).

[10] H. Kahn, "Applications of Monte Carlo," Technical Report AECU-3259 (1956).

[11] L. Koblinger, "Direct Sampling from the Klein–Nishina Distribution for Photon Energies Above 1.4 Mev," *Nucl. Sci. Eng.*, **56**, *2*, 218 (1975).

[12] C. J. Everett, "A third Monte Carlo sampler: (a revision and extension of samplers I and II)," Technical Report LA-9721-MS, Los Alamos National Laboratory (1983).

[13] P. Virtanen, R. Gommers, T. E. Oliphant, M. Haberland, T. Reddy, D. Cournapeau, E. Burovski, P. Peterson, W. Weckesser, J. Bright, S. J. van der Walt, M. Brett, J. Wilson, K. J. Millman, N. Mayorov, A. R. J. Nelson, E. Jones, R. Kern, E. Larson, C. J. Carey, İ. Polat, Y. Feng, E. W. Moore, J. VanderPlas, D. Laxalde, J. Perktold, R. Cimrman, I. Henriksen, E. A. Quintero, C. R. Harris, A. M. Archibald, A. H. Ribeiro, F. Pedregosa, P. van Mulbregt, and SciPy 1.0 Contributors, "SciPy 1.0: Fundamental Algorithms for Scientific Computing in Python," *Nature Methods*, **17**, 261 (2020).

[14] R. Ribberfors and K. F. Berggren, "Incoherent-x-ray-scattering functions and cross sections by means of a pocket calculator," *Physical Review A*, **26**, *6*, 3325 (1982).

[15] J. Persliden, "A Monte Carlo program for photon transport using analogue sampling of scattering angle in coherent and incoherent scattering processes," *Computer Programs in Biomedicine*, **17**, *1-2*, 115 (1983).

[16] J. H. Hubbell, W. J. Veigele, E. A. Briggs, R. T. Brown, D. T. Cromer, and R. J. Howerton, "Atomic form factors, incoherent scattering functions, and photon scattering cross sections," *Journal of Physical and Chemical Reference Data*, **4**, *3*, 471 (1975).

[17] A. Robinson, "Development and Implementation of Continuous Energy Adjoint Monte Carlo Methods for Photons," PhD Thesis, University of Wisconsin - Madison (2019).

[18] K. Mathews, "Random Sampling from the Klein-Nishina Distribution: Efficiency, Parsimony, and Speed," *Nuclear Science and Engineering*, **173**, *3*, 207 (2013).